FERMILAB-PUB-76-153-E

Nuclear reactions of ^{197}Au with 11.5- and 300-GeV protons*

S. B. Kaufman, M. W. Weisfield,† E. P. Steinberg,
B. D. Wilkins, and D. Henderson
Chemistry Division, Argonne National Laboratory
Argonne, Illinois 60439

The formation cross sections of more than 60 nuclides produced in the reaction of 11.5- and 300-GeV protons with ^{197}Au were measured. Most of the measurements were done by direct counting of the target with calibrated Ge(Li) γ-ray spectrometers and spectral analysis with computer programs. In addition, chemical separations of osmium and gold fractions permitted the assay of nuclides which could not be resolved in the unseparated targets. The cross-section ratio at the two energies, $\sigma_{300}/\sigma_{11.5}$, was within 20% of unity for all nuclides studied, which ranged in mass from ^{22}Na to ^{196}Au. This is interpreted as showing that the spectrum of excitation energies left in the nucleus is nearly independent of bombarding energy above ∿ 10 GeV. The small cross section changes observed are shown to be continuations of trends seen previously at lower energies.

---

*Work performed under the auspices of the U. S. Energy Research and Development Administration.

†Present address: Radiation Management Corp., Philadelphia, Pa.

Charge dispersion curves were estimated with the aid of an empirical formula, and a mass-yield curve was constructed.

[NUCLEAR REACTIONS ^{197}Au + 11.5-, 300-GeV protons; measured σ for formation of 63 nuclides from ^{22}Na to ^{196}Au; estimated charge dispersions and mass yield curve.
RADIOACTIVITY measured $T_{1/2}$ of ^{182}Os, ^{183}Os, $^{183}Os^{m}$]

I. INTRODUCTION

As part of a program to study the interactions of high-energy protons with complex nuclei several comparisons of formation cross sections at 300 GeV and at lower energies have been made recently. For targets of vanadium,[1] cobalt,[1] silver,[2-4] gold,[5] and uranium[6-8] the cross sections of most products measured were essentially the same between proton energies of 11.5 and 300 GeV. With the exception of uranium, the ratio $\sigma_{300}/\sigma_{11.5-29}$ was unity to within 10%. However, that ratio was significantly lower for products in the mass region $70 < A < 140$ formed from uranium.[6] Although the difference is small, it was felt desirable to further investigate these cross-section ratios for a heavy element target. Gold was chosen as the target element because the absence of appreciable low-excitation-energy fission makes the high-energy processes more prominent.

In order to measure cross sections efficiently for a large variety of products, the technique of non-destructive analysis of the target using high-resolution γ-ray spectroscopy was chosen. This technique has been used successfully to study low-energy fission of uranium,[9-11] photofission of heavy elements up to 1 Gev,[12-14] and fission of gold by 580-MeV protons.[15] Of the previous cross section comparisons at 300 GeV, this method was also used for vanadium,[1] cobalt,[1] and silver,[2-4] but for gold[5] and uranium[6-8] selected elements were chemically separated, because of the much larger number of nuclides formed and the resulting complexity of the spectra. However, it has been established[16] that long-lived nuclides can be satisfactorily resolved from heavy targets bombarded with GeV protons after a suitable decay period, and with care some short-lived nuclides with prominent γ-rays can be determined, such as ^{24}Na and ^{28}Mg from gold and uranium targets bombarded with GeV protons.[17]

In addition to measuring the cross section ratios at 11.5 and 300 GeV, it was also desired to investigate the charge dispersion curves for the products in different mass regions, in conjunction with a concurrent study[18] of the average recoil properties of many of the same nuclides. Knowledge of such charge dispersions are required to estimate the mean atomic number of precursor nuclei to the product measured, in order

to calculate the mean kinetic energy from the mean range. In connection with the recoil study chemical separations of osmium and gold fractions were made, and thus the cross section measurements for the nuclides ^{185}Os, ^{194}Au, and ^{196}Au made by gross γ-ray spectroscopy could be checked against those made on chemically separated samples. In addition, the nuclides ^{182}Os, ^{183}Os, and $^{183}Os^{m}$, which could not be resolved in the gross γ-ray measurements, could also be determined.

II. EXPERIMENTAL PROCEDURE

The irradiations at 11.5 GeV were performed in the internal circulating proton beam of the Argonne National Laboratory Zero Gradient Synchrotron (ZGS). Targets consisted of three aluminum monitor foils (each of 7 mg cm^{-2} thickness) upstream of three gold target foils (each of 24 mg cm^{-2} thickness). Before the irradiation the leading edge of the target stack was carefully cut to insure alignment; after the irradiation the stack was cut 1 cm back from the leading edge and the center aluminum and gold foils were weighed to determine their exact thickness prior to counting. The irradiations at 300 GeV were performed in the Meson Hall external proton beam at the Fermi National Accelerator Laboratory (Fermilab). Similar target stacks to those described above were enclosed in evacuated polyethylene bags, and after the irradiation a portion of the stack centered on the beam spot was cut out.

The center foils were used in order that recoil loss be compensated. With the thicknesses used in this experiment the compensation was complete for all nuclides of interest[17,18] with the exception of ^{7}Be. In the latter case the kinetic energy spectrum of the recoils extends to several hundred MeV[19,20] and foils much thicker than used here would be necessary to completely compensate for loss. This was borne out by the cross sections observed in this work for ^{7}Be at 11.5 and 300 GeV, which were both about 30% lower than that measured at 30 GeV,[21] in which much thicker targets were used.

A total of five irradiations with the total proton intensity varying from ca. 1×10^{15} to 3×10^{16} were carried out at each energy. Lengths of irradiations varied from 2 to 40 minutes at the ZGS and from 0.5 to 48 hours at the Fermilab. The single 48-hour irradiation was only used to assay nuclides with half-lives greater than about 10 days. Saturation corrections were made in all cases, taking account of periods of varying beam intensity.

The proton flux was determined by assaying the aluminum monitor foil for ^{24}Na, using both a β-γ coincidence counter and the same calibrated Ge(Li) detectors used for counting the gold targets. The agreement between the two methods was always within 2%. The disintegration rate of ^{24}Na was corrected for secondary effects by reducing it by 7%, since the effect was measured in a separate experiment to be 10% per 100 mg cm^{-2}

of gold target downstream of the monitor. This value is in good agreement with other such measurements.[6,22,23] The monitor cross section at 11.5 GeV was taken to be 8.6 mb.[24] In previous work[1-8] at 300 GeV the monitor cross section was assumed to be the same at both energies. It has recently been measured at 300 GeV[25] relative to the $^{12}C(p,pn)^{11}C$ cross section, whose absolute cross section has now been measured.[26] Using the value for the latter reaction cross section of 24.6 ± 1.6 mb at 300 GeV and the measured[25] ratio of 0.33 ± 0.01, one calculates a monitor cross section for ^{24}Na from aluminum of 8.1 ± 0.6 mb. Since this value is the same within experimental error as the 8.6 mb value used in previous work, and in order to be consistent with that work, we will also use the value 8.6 mb at 300 GeV.

The gold targets were counted on one of two Ge(Li) spectrometers with 4096-channel capacity and magnetic tape readout. The two detectors used both had resolutions of 2.0 keV (FWHM) at 1332 keV; their efficiences relative to NaI were 6% and 10%. A source distance of 10 cm was used, making summing of coincident γ-rays negligible, and the detectors were calibrated for absolute efficiency with a variety of standards over the energy range 88-2754 keV. Based on the deviations of individual calibration points from a smooth curve we estimate the absolute accuracy of the calibrations to

be $\pm$ 5%. A precision pulser was used to determine the counting losses due to pulse pileup, which were appreciable for the early counts.

Spectra were recorded periodically, starting from 5 h to 5 days after the bombardment, depending on the total proton intensity, and measurements continued for as long as 2 years. The spectra were analyzed with the aid of two computer programs, SAMPO[27] and GAMANAL.[28] In addition, all of the spectral peaks of interest were visually examined for indications of more than one γ-ray, such as shoulders, asymmetric shape, or abnormal width. The two different computer programs usually gave good agreement for the peak areas of those peaks which were single and well-separated from neighbors. The GAMANAL program proved to be better than SAMPO in resolving close multiplet structure, as shown by the better resulting decay curves and agreement of measured intensities with literature values for γ-rays from the same nuclide.

Peaks in the spectra were identified and assigned to specific nuclides on the basis of energy and half-life. For each peak of interest the calculated photon intensity as a function of time was used as input to a weighted least-squares decay-curve resolution program (CLSQ),[29] using as weights the values of $1/\sigma_i^2$ for each data point, with the standard deviation σ_i given by the spectral analysis program. The literature value of the half-life of the assumed nuclide was used, and a

poor fit of the data to that half-life was grounds for rejection of the peak, unless it could be established that a known nuclide was also contributing to the peak. In that case, the second nuclide's half-life was included in the decay-curve resolution, and the intensity of the interfering γ-ray was required to be in agreement with other γ-rays from that nuclide, if any. If the half-lives of two such nuclides differed by less than about a factor of three, no clear resolution of the decay curve could be made, and the peak was rejected. In many cases genetically related nuclides were thus eliminated, although their γ-rays were intense and well-resolved, for example 85-day ^{88}Zr and 108-day ^{88}Y.

Table I lists the nuclides whose cross sections could be determined, their half-lives, the γ-rays used and their abundances, and also identifies in the footnotes any interfering γ-rays for which decay-curve resolutions were performed. In addition there is given for each nuclide a "reliability grade", based on the above considerations. A grade of A indicates a nuclide with two or more γ-rays which both showed single-component decay curves and whose observed relative intensities agreed with the literature values. In this context, a peak due to a long-lived nuclide which decayed with the correct half-life after short-lived interferences had decayed away was classed as a single-component decay curve. A grade of B indicates a

nuclide for which only one γ-ray could be used and which exhibited a single-component decay curve, or a nuclide with two γ-rays requiring decay-curve resolution and whose intensities agreed. A grade of C indicates nuclides with only one γ-ray which required resolution of the decay curve.

Three of the nuclides listed in Table I were not resolved in the gross γ-ray spectra but rather in chemically separated osmium samples, ^{182}Os, $^{183}Os^{g}$ and $^{183}Os^{m}$, and are denoted by "chem" in this column. The half-lives for ^{182}Os and $^{183}Os^{m}$ listed were measured in this work by following the decay of the listed γ-rays. The experimental values found were 22.0 ± 0.2 h for ^{182}Os and 9.1 ± 0.2 h for $^{183}Os^{m}$. The intensity of the 381.8-keV γ-ray of $^{183}Os^{g}$ decayed with an apparent half-life of 14.5 ± 0.3 h; this is a resultant of the combined growth and decay of the ground state from the isomeric state and its independent decay. Assuming a 16% branch for the isomeric transition[30] and using the value of 9.1 h for the half-life of the isomeric state, the calculated half-life of the ground state is 14.0 ± 0.8 h. The cross section for $^{183}Os^{g}$ was then calculated taking into account the partial feeding from $^{183}Os^{m}$. Nearly equal cross sections for the two states were found, in agreement with the isomer ratio resulting[31] from decay of ^{183}Ir.

III. RESULTS

A cross section was calculated for each nuclidic γ-ray and each bombardment, based on the end-of-bombardment (EOB) photon intensity and the abundance as given in Table I. At least three bombardments at each energy were included for each nuclide. In most cases the EOB photon intensity of a given photon in different bombardments had similar percentage standard deviations, as given by the least-squares decay-curve program, and the scatter of the individual cross sections calculated from these intensities was consistent with those standard deviations. Therefore, an unweighted average cross section was computed for each γ-ray, together with the standard deviation of the average, calculated as $(\Sigma\Delta_i^2)^{1/2}/(N-1)^{1/2}$, where Δ_i is the deviation of the i'th measurement from the average and N is the number of measurements. An "internal" standard deviation was also calculated, $\sigma = (1/\Sigma\sigma_i^2)^{1/2}$, where σ_i is the standard deviation of the i'th measurement, derived from that of the photon intensity. The larger of the two numbers was used as the standard deviation of that cross section, and in cases where two or more γ-rays were used, the final cross section was calculated as a weighted average of the cross sections for each γ-ray.

In addition, the following estimated errors were folded in quadratically to obtain the error listed for each cross section:

5% uncertainty in the absolute efficiency calibrations of the detectors, and 2% uncertainty in the secondary correction for ^{24}Na in the monitors. Uncertainties in the γ-ray abundances were not included separately since agreement between the observed relative intensities and the literature values was one of the requirements for the acceptability of the γ-rays for cross section determinations, as discussed above.

In calculating the cross section ratios, $\sigma_{300}/\sigma_{11.5}$, the ratio was calculated separately for each γ-ray so that errors in efficiency and abundance would cancel out. Moreover, only those data taken with the same detector were compared, eliminating another source of error.

The results of these measurements are presented in Table II, which gives for each nuclide the cross section at 11.5 GeV and the cross section ratio, $\sigma_{300}/\sigma_{11.5}$, at the two energies. Also given for each nuclide is the type of yield (C = cumulative; I = independent) and any previous cross section measurements with a gold target[5,15,32-29] for comparison with the present measurement.

With a few exceptions the cross sections measured here are in satisfactory agreement with previous measurements at proton energies above 10 GeV. This agreement supports the conclusion that the technique of gross γ-ray spectroscopy without chemical separation can be used to assay a large number of nuclides in the complex mixture produced when GeV protons interact with

heavy targets. The exceptions to this agreement are the rare-earth nuclides measured by Bächmann[38] at 28 GeV, for which satisfactory agreement is found only for ^{139}Ce. For the nuclides ^{145}Eu, ^{147}Eu, ^{146}Gd, and ^{149}Gd, Bächmann's cross sections are lower than those measured here at 300 GeV by ratios of 0.5-0.8. However, a subtractive correction was applied to the cross sections for these nuclides by Bächmann in order to correct for their formation by α-decay from short-lived heavier rare earths. If such a correction were made to the present data, the agreement between the two experiments would be improved.

The discrepancy is in the opposite direction for ^{148}Eu, for which Bächmann's cross section is twice as large as that measured here. Because the cross section for this nuclide is independent and thus helps delineate the charge dispersion curve in this mass region, it is an important measurement. Both experimental values have been included in the charge dispersion data in Fig. 3, where it is seen that the empirical equation discussed below is in good agreement with the measurement of Bächmann. It is possible that the 550.2-keV γ-ray of ^{148}Eu was not correctly resolved from the nearby 552.5-keV γ-ray of ^{83}Rb, which was twice the intensity.

For bombarding energies below 10 GeV, the data in Table II show that most nuclides have lower cross sections. The exceptions are the medium mass (A ≈ 90) neutron excess nuclides

^{84}Rb, ^{95}Nb and ^{103}Ru, whose cross sections are the same or larger at ∿ 0.5 GeV than at 11.5 GeV. In addition, the (p,pn) reaction product, ^{196}Au, has essentially the same cross section at 0.4 GeV as at 11.5 GeV. These trends with energy are discussed more fully in the next section.

IV. DISCUSSION

A. Energy variation of cross sections

The experimental ratios of the cross sections at 300 GeV to those at 11.5 GeV, $\sigma_{300}/\sigma_{11.5}$, are shown as a function of mass number in Fig. 1. Nuclides for which the error in the ratio is greater than 20% have been omitted from Fig. 1 for clarity. The data of Yu and Porile[5] for the same energies and target have been included, and separate symbols have been used to denote independent and cumulative cross sections and to distinguish neutron-excess and neutron-deficient nuclides. It is seen that the cross section ratio varies regularly with mass number, decreasing from about 1.1 for the lightest nuclides measured to about 0.9 for nuclides in the mass range $121 \leq A \leq 185$. The ratio then increases to values of 1.0-1.2 for nuclides close to the target. Although the absolute value of these ratios is uncertain to the extent of the uncertainty in the absolute values of the monitor cross section, the variations of the ratio would be unaffected by such uncertainty. These data

on gold cross sections confirm the observations of Chang and Sugarman[6] for a uranium target that $\sigma_{300}/\sigma_{11.5}$ averaged 1.03 ± 0.14 for products of $45 \leq A \leq 67$ and decreased to 0.81 ± 0.14 for products of $83 \leq A \leq 140$.

These general trends are of some interest and will be discussed in more detail below, but the striking fact is that the individual cross sections for a wide range of products change so little between 11.5 and 300 GeV incident proton energy. This observation has been commented on previously,[1-8] with the conclusion that the spectrum of excitation energies deposited in the nucleus is essentially independent of bombarding energy above 10 GeV. The increased number of pions and other hadrons produced in nucleon-nucleon collisions at the higher energy must escape the nucleus without multiplying the intranuclear cascade.

There is considerable evidence from studies of charged-particle multiplicities in proton-nucleus[39,40] and pion-nucleus[41] interactions that at multi-GeV energies there is no cascading of the secondary hadrons inside the nucleus. The average multiplication of particles inside the nucleus is measured by $R_A = \langle n \rangle_A / \langle n \rangle_p$, where $\langle n \rangle_A$ is the average number of charged relativistic (shower) particles produced in a hadron-nucleus interaction, and $\langle n \rangle_p$ is the number of charged secondaries in the corresponding hadron-proton collision. The quantity R_A is only weakly dependent on

incident energy in the GeV region and becomes energy independent above 60 GeV.[41,42] The increase of R_A with target mass is also small, with most of the increase due to particles produced at large angles.[39,41] The forward relativistic particles, in contrast, have the same multiplicity for a heavy nucleus as for hydrogen.[41]

These observations suggest[43] that at ultra-relativistic energies the hadron state produced in the first interaction acts like a single hadron while traversing the nucleus, and does not decay to its final multi-particle state until after it has left the nucleus. Under these circumstances one would expect that at sufficiently high energies the cross sections and recoil properties of nuclides resulting from hadron-nucleus interactions would approach asymptotic values. Although cross-section measurements alone may not be the most sensitive test of these ideas, the near constancy of cross sections above 10 GeV suggests that the asymptotic region may have been reached. There is evidence[17,18,44] that the recoil properties of certain nuclides formed from heavy targets are still changing between 11.5- and 28-GeV incident energy, and only approach limiting values at 300 GeV.

The small changes in cross section values between 11.5- and 300 GeV are mainly continuations of the trends observed at lower energy. Although there has been no comprehensive study

of the energy variation of cross sections with heavy targets since the early work at the Cosmotron,[45] it is possible to make some generalizations. In the fragmentation region of masses ($A \lesssim 50$) the formation cross sections from heavy targets rise rapidly above a threshold of about 0.5 GeV,[35,45-47] leveling off in the multi-GeV region. The observed ratios in this work of $\sigma_{300}/\sigma_{11.5}$ = 1.07-1.13 for these light nuclides are consistent with such a leveling off above 10 GeV. On the other hand, the heavier neutron-deficient nuclides, with $120 \leq A \leq 190$, have characteristic spallation-like excitation functions, which go through a maximum and then decrease with increasing bombarding energy.[48-50] The energy at which the cross section peaks is higher the farther the product is from the target in mass, but all such products are apparently over the peak at an energy of 11.5 GeV, and show a further small decrease in going to 300 GeV.

Most of the nuclides in the middle-mass region have the same cross section at 11.5 and 300 GeV, and probably are formed by a mixture of mechanisms in which the two energy dependences described above are combined and cancel out. The exceptions to this are the neutron-excess medium-mass nuclides (^{95}Nb, ^{103}Ru) whose cross sections decrease monotonically above about 0.5 GeV. They are formed primarily by binary fission at low bombarding energies, and the contribution of that process to their formation decreases with increasing energy. Since the total binary fission

cross section remains approximately constant above 0.5 GeV,[51] the charge distribution must shift toward more neutron-deficient nuclides at higher energies, in order to compensate for the decreasing cross sections of the neutron-excess nuclides.

The cross sections for nuclides close to the target are the same or larger at 300 GeV as at 11.5 GeV. In particular, the nuclides ^{190}Ir and ^{192}Ir show a 20% increase in cross section at the higher energy. It may be significant that these are independent cross sections, as is that of ^{188}Ir, which also has a larger cross section, although with a large error. Since a charge dispersion curve is determined by such independent cross section values, a possible interpretation of these ratios is that the charge dispersion curves are shifted more toward neutron-excess nuclides at 300 GeV than at 11.5 GeV. This could arise, for example, from an increased probability of emission of positively charged particles as compared to neutral or negatively charged particles in the intranuclear cascade, since the evaporation sequence is most likely independent of incident energy.

B. Charge dispersions and empirical cross-section formulae

As stated in the Introduction, one of the aims of these measurements was to construct representative charge-dispersion curves for different mass regions, in order to allow the

calculation of the atomic number of the average precursor for a given nuclide. This could then be used to relate the experimental mean range for that nuclide to the mean kinetic energy at formation.

Unfortunately there is insufficient data on independent cross sections in any local region to construct such charge dispersion curves. This has been done for gold as a target only at mass number A = 131 at 11.5 and 300 GeV,[5] near A = 148 at 28 GeV,[38] and at A = 72 at 2.9 GeV.[34] It was decided to use the available data and fit the parameters of an empirical formula, then use that formula to estimate the unmeasured cross sections. The formula used was first suggested by Rudstam[52] and is his "CDMD" equation:

$$\sigma(Z,A) = \sigma_o \exp[PA-R|Z-SA+TA^2|^{3/2}] \qquad (1)$$

where $\sigma(Z,A)$ is the independent cross section for the nuclide of atomic number Z and mass number A, and P, R, S, and T are empirical parameters. Rudstam fit equation (1) to a large body of spallation data and found how the parameters varied with incident energy and target mass. Most of the data used for the fit was for medium-weight target elements (Z = 23-47), and the equation was intended to apply only to spallation products and not to nuclides formed by fission or fragmentation of heavy targets. Furthermore, while the form of equation (1) results

in symmetric charge disperion curves, the experimental evidence for GeV protons interacting with heavy targets (e.g. Ta[53], Au[5,34,38] and Pb[54,55]) is that they are asymmetric.

Nevertheless, the cross section data of this work, together with previous measurements[5,36-38] at 11.5 -29 GeV, were used in an attempt to fit the parameters of equation (1). It was found that a satisfactory fit could be obtained by separating the data into two mass regions; these correspond approximately to a spallation region ($120 \lesssim A \lesssim 190$) and to a medium-mass region with contributions from fission, deep spallation and fragmentation ($40 \lesssim A \lesssim 105$). The parameters of equation (1) for these two mass regions which gave the best fit to the experimental cross sections are given in Table III, with the values found by Rudstam[52] for comparison.

Charge dispersion curves calculated with these values of the parameters for particular mass numbers are shown in Figs. 2 and 3, with experimental cross sections for nuclides close to those mass numbers. The most probable charge, Z_p, was calculated for each mass number from the equation

$$Z_p = SA-TA^2 \tag{2}$$

and the experimental cross section for each isobar was plotted at the corresponding value of Z_p-Z. The dashed curves in

Figs. 2 and 3 show how the cumulative cross sections behave for positron/electron-capture decay. In Fig. 3, the cross sections for ^{145}Eu, ^{147}Eu, ^{149}Eu, ^{146}Gd, and ^{149}Gd have been corrected for the contribution to their cross section from α-decay of the A + 4 nuclides, using equation (1) to estimate the formation cross sections of the latter. The data of Bächmann[38] has already been corrected in this way.

The quality of fit of the data to equation (1) in the two regions of mass is seen to be adequate for the purpose of estimating the atomic number of the average precursor of a given nuclide, and equation (1) provides a simple formulation for estimating unmeasured cross sections. The dependence of the parameters R, S, and T on mass number is shown in Fig. 4, where the present fit is given by the solid lines in the two mass regions, and the values given by Rudstam[52] are the dashed lines. Figure 4a shows that R is smaller in the present fit than in Rudstam's, resulting in wider charge dispersions. This is especially true near A = 100, where the wide charge dispersion is due to the contribution of different reaction mechanisms, namely spallation and fission. Figure 4b shows the ratio Z_p/A, which is linear in A according to equation (2), and in addition the trend of beta stability is shown as the dotted curve. It is seen that the most probable charge Z_p for a given mass is larger for the present set of parameters

than for Rudstam's in the spallation region, i.e., more neutron deficient, but is smaller in the lighter mass region, i.e., closer to stability. These differences are probably due to the fact that the present fit is restricted to GeV protons on gold, while Rudstam's fit made use largely of data from lighter elements.

C. Mass-yield curve

In the spallation region, A $\geq$ 120, the cumulative cross sections represent very nearly the total cross section at a given mass number, with the exception of the mass region near A = 148, where α-decay depletes the yield at some masses and enhances others. These cumulative cross sections thus are useful in establishing the mass-yield curve in this mass region. However, in the lighter mass region this is not generally true, since there are appreciable cross sections for forming stable and neutron-excess nuclides, and the neutron-deficient cumulative yields no longer represent most of the isobaric cross section. The best measurements to help delineate the mass-yield curve in this region are those of Hudis, *et al.*,[36] who measured the total isobaric cross sections at A = 20, 21, 22, 38, 83 and 131 by determining the cumulative yields of the stable rare-gas isotopes. Figure 5 shows these data, together with cumulative cross sections from Table II and Ref. 5 at 11.5 GeV. Although

the cross sections for ^{196}Au and ^{194}Au are independent, they probably represent the major part of the yield at those mass numbers, and thus are included in Fig. 5. For comparison the two solid lines indicate the mass yield calculated from equation (1) with the parameter values in Table III, while the dashed lines indicate the likely extrapolations to the lighter masses and the region close to the target. Of the medium-mass nuclides, only ^{83}Rb and ^{87}Sr appear to cumulate the major portion of the yield. As stated above, near A = 148 the cumulative cross sections are larger than the mass-yield curve would indicate because of feeding by α-decay.

V. SUMMARY AND CONCLUSIONS

The technique of identifying and measuring the intensities of γ-rays in a complex mixture of radionuclides by high-resolution Ge(Li) spectroscopy was used to study the reactions of high-energy protons with ^{197}Au. Cross sections for the formation of more than 60 nuclides were determined for bombarding energies of 11.5 and 300 GeV. The ratio of cross sections at the two energies, $\sigma_{300}/\sigma_{11.5}$, varies in a regular way with the product mass number, but does not deviate from unity by more than 20% for any of the products measured here. This is in agreement with the results of previous studies[1-8] at 300 GeV, and leads to the conclusion that the distribution of excitation energies deposited in the nucleus changes very little over the energy range 11.5-300 GeV.

This is supported by measurements of charged-particle multiplicity in hadron-nucleus interactions[39-41] above $\sim$ 60 GeV, which show that the intranuclear cascade is not multiplied by secondary hadrons inside the nucleus. Because of this the increase in secondary production with energy does not cause a corresponding increase in the excitation energy transferred to the nucleus by the cascade, and the excitation-energy spectrum should approach an asymptotic distribution above $\sim$ 60 GeV. The small changes in cross sections between 11.5 and 300 GeV which are observed are shown to be continuations of trends previously observed at lower energies.

The Rudstam[52] empirical cross section formula for spallation products was used to systematize the cross section values at 11.5 GeV by fitting the parameters separately for two mass regions. In spite of the experimental observation that charge dispersions are not symmetric, the symmetric form of the empirical equation gives a reasonable fit to the independent cross section data. A mass-yield distribution was estimated with the aid of this equation and a number of cumulative cross sections for products of mass number $A \geq 120$.

TABLE I. Decay properties of observed nuclides.[a]

Nuclide	$T_{1/2}$	Observed γ-ray (keV)	Abundance	Reliability Grade[b]
^{22}Na	2.62 yr	1274.5	1.00	B
^{24}Na	15.03 h	1368.5	1.00	A
		2753.9	1.00	
^{28}Mg	20.93 h[c]	1778.9(^{28}Al)[d]	1.00	B
^{42}K	12.4 h	1524.7	0.18	B
$^{44}Sc^{m}$	2.44 day	1157.0(^{44}Sc)	1.058[e]	B
^{46}Sc	83.8 day	889.3	1.00	A
		1120.5	1.00	
^{48}V	15.97 day	983.5	1.00	A
		1312.1	0.97	
$^{52}Mn^{g}$	5.7 day	1434.3	1.00	B
^{54}Mn	312.5 day	834.8	1.00	B
^{59}Fe	44.6 day	1099.2	0.565	A
		1291.6	0.432	
^{56}Co	77.3 day	846.8	1.00	B
^{58}Co	71.3 day	810.8[f]	0.99	C
^{60}Co	5.26 yr	1173.2	1.00	A
		1332.5	1.00	
^{65}Zn	244 day	1115.5	0.508	B
$^{69}Zn^{m}$	13.76 h[c]	438.7	0.95	B
^{74}As	17.77 day	595.9	0.592	B
^{75}Se	120 day	264.7	0.573	B
		279.5[g]	0.248	
^{83}Rb	86.2 day	529.5	0.304	A
		552.5	0.165	
^{84}Rb	33 day	881.5[h]	0.734	C

TABLE I. (continued)

Nuclide	$T_{\frac{1}{2}}$	Observed γ-ray (keV)	Abundance	Reliability Grade[b]
^{83}Sr	32.4 h	762.5	0.332[i]	B
^{87}Y	80.3 h	388.4($^{87}Sr^{m}$)	0.855[e]	A
		484.8	0.992[j]	
^{89}Zr	78.5 h	909.2	1.00	B
^{90}Nb	14.6 h	2319.2	0.82	B
^{95}Nb	35.1 day	765.8[k]	0.99	C
^{96}Tc	4.3 day	849.9	0.98	B
^{103}Ru	39.6 day	497.1[l]	0.90	C
^{100}Rh	20 h	1553.5[m]	0.28	B
		2376.1[m]	0.446	
^{100}Pd	4.0 day	1553.5[m](^{100}Rh)	0.28	B
		2376.1[m](^{100}Rh)	0.446	
^{105}Ag	41.29 day[c]	280.4[g]	0.32	C
$^{120}Sb^{m}$	5.8 day	1023.2	0.99	B
^{121}Te	16.8 day[n]	573.1[o]	0.80	C
$^{121}Te^{m}$	154 day	212.2	0.89	B
^{122}Xe	20.0 h	564.0(^{122}I)	0.177	B
^{127}Xe	36.4 day	172.1[p]	0.247[q]	B
		202.8[r]	0.681[q]	
^{131}Ba	11.7 day	123.7	0.28[s]	B
		496.2[l]	0.48[s]	
^{133}Ba	10.9 yr	355.9	0.67	B
^{139}Ce	137.2 day	165.8	0.804[t]	B
^{143}Pm	265 day	742.0	0.385[u]	B
^{144}Pm	360 day	618.0	1.00	B
^{145}Eu	5.93 day[u]	893.7	0.475	B

TABLE I. (continued)

Nuclide	$T_{1/2}$	Observed γ-ray (keV)	Abundance	Reliability Grade[b]
^{147}Eu	24.5 day[v]	601.4	0.060	A
		677.5	0.090	
^{148}Eu	54.9 day[v]	550.2	0.99	B
^{149}Eu	93.1 day[u]	277.2	0.036[v]	A
		327.7	0.040[v]	
^{146}Gd	48.3 day	114.7 + 115.5	0.91	A
		633.4 + 634.2 (^{146}Eu)	0.90[e]	
		747.1 (^{146}Eu)	1.08[e]	
^{149}Gd	9.4 day	149.6	0.426	A
		298.5	0.232	
^{167}Tm	9.25 day[w]	207.9	0.43	B
^{169}Yb	32 day	177.2	0.218	B
^{170}Lu	2.15 day	2126.1	0.052	A
		2691.5	0.023	
		2748.2	0.022	
		2845.3	0.018	
^{171}Lu	8.3 day	667.6	0.12[x]	A
		739.8	0.48[x]	
^{173}Lu	1.37 yr	272.4	0.18	B
^{172}Hf	1.87 yr[y]	181.4 (^{172}Lu)	0.199	A
		810.0[f] (^{172}Lu)	0.158	
		912.1 (^{172}Lu)	0.147	
		1093.5 (^{172}Lu)	0.636	
^{175}Hf	70 day	343.4	0.85	B
^{183}Re	70 day	162.3	0.26[z]	B
^{182}Os	22.0 h[aa]	180.2	0.37[bb]	Chem.
^{183}OS	14.0 h[aa]	381.8	0.78[z]	Chem.

TABLE I. (continued)

Nuclide	$T_{\frac{1}{2}}$	Observed γ-ray (keV)	Abundance	Reliability Grade[b]
$^{183}Os^{m}$	9.1 h[aa]	1102.0	0.50[z]	Chem.
		1108.0	0.23[z]	
^{185}Os	93.6 day	646.1	0.813	B
^{188}Ir	41.5 h	2214.6[cc]	0.13	C
^{190}Ir	12.1 day[dd]	407.2	0.262[dd]	A
		557.8	0.273[dd]	
		605.3	0.382[dd]	
^{192}Ir	74.0 day	295.9	0.291	A
		316.5	0.831	
		468.1	0.476	
^{188}Pt	10.2 day	195.1	0.18	A
		2214.6[cc] (^{188}Ir)	0.157[e]	
^{194}Au	39.5 h	328.5	0.591	B
^{196}Au	6.18 day	333.0	0.238	A
		355.7	0.88	

[a] Half-lives and abundances taken from the compilation of W.W.Bowman and K. W. MacMurdo, Atomic Data and Nuclear Data Tables 13, 89 (1974), unless otherwise indicated.

[b] Defined in text.

[c] S. J. Rothman, N. L. Peterson, W. K. Chen, J. J. Hines, R. Bastar, L. C. Robinson, L. J. Nowicki, and J. B. Anderson, Phys. Rev. C9, 2272 (1974).

[d] Daughter radiation.

[e] Includes factor for genetic relationship.

[f] Two-component decay (^{58}Co and ^{172}Hf).

[g] Two-component decay (^{75}Se and ^{105}Ag).

[h] Two-component decay (^{84}Rb and ^{185}Os, 880.3 - keV γ).

[i] R. C. Etherton, L. M. Beyer, and W. H. Kelly, Phys. Rev. 168, 1249 (1968).

[j] W. H. Zoller, W. B. Walters, and C. D. Coryell, Phys. Rev. 185, 1537 (1969).

[k] Two-component decay (^{95}Nb and $^{102}Rh^m$, 766.8 - keV γ). ^{95}Zr parent not observed.

[l] Two-component decay (^{103}Ru and ^{131}Ba).

[m] Parent-daughter decay ($^{100}Pd \rightarrow {}^{100}Rh$).

[n] H. M. A. Karim, Radiochim. Acta 19, 1 (1973).

[o] Parent-daughter decay ($^{121}Te^m \rightarrow {}^{121}Te$).

[p] Two-component decay (^{127}Xe and ^{173}Lu, 171.5 - keV γ).

[q] R. Collé and R. Kishore, Phys. Rev. C9, 981 (1974).

[r] Two-component decay (^{127}Xe and ^{172}Hf, 203.3 - keV γ).

[s] C. M. Lederer, J. M. Hollander, and I. Perlman, Table of Isotopes (Wiley, New York, 1967), 6th ed.

[t] J. Legrand, M. Blondel, and P. Magnier, Nucl. Instr. Methods 112, 101 (1973).

[u] Y. Y. Chu, E. M. Franz, and G. Friedlander, Phys. Rev. C1, 1826 (1970).

[v] D. R. Nethaway, B. Mendoza, and R. S. Newbury, Phys. Rev. C12, 1310 (1975).

[w] P. J. Karol, J. Inorg. Nucl. Chem. 32, 2817 (1970).

[x] D. Barneoud, J. Boutet, J. Gizon, and J. Valentin, Nucl. Phys. A138, 33 (1969).

[y] Y. Y. Chu and P. J. Karol, Inorg. Nucl. Chem. Lett. 7, 1205 (1971).

[z] Ref. 30

[aa] Measured in this work.

[bb] S. B. Burson, P. J. Daly, P. F. A. Goudsmit, and A. A. C. Klaasse, Nucl. Phys. A204, 337 (1973).

[cc] Parent-daughter decay ($^{188}Pt \rightarrow {}^{188}Ir$).

[dd] Nuclear Data Sheets 9, 401 (1973).

TABLE II. Cross sections from interaction of 11.5-GeV protons with ^{197}Au, cross section ratios $\sigma_{300}/\sigma_{11.5}$, and previous measurements.

Nuclide	Type of Yield[a]	$\sigma_{11.5}$ (mb)	$\sigma_{300}/\sigma_{11.5}$	Previous measurements σ (mb)	Ep (GeV)	Ref.
^{22}Na	C	2.52±0.15	1.09±0.03	2.10±0.3	30	b
^{24}Na	C	12.7±1.0	1.10±0.07	10.4±1.2	30	b
^{28}Mg	C	3.03±0.22	1.07±0.06			
^{42}K	I	3.6±0.5	1.08±0.11			
$^{44}Sc^{m}$	I	1.57±0.13	1.11±0.08	1.64±0.12	18.2	c
^{46}Sc	I	4.60±0.30	1.07±0.04	0.075±0.019	0.58	d
				4.42±0.36	18.2	c
^{48}V	C	1.56±0.12	1.13±0.07			
$^{52}Mn^{g}$	I	1.19±0.07	1.09±0.04			
^{54}Mn	I	4.09±0.26	1.05±0.04	0.181±0.075	0.58	d
^{59}Fe	C	1.69±0.13	1.02±0.05	0.16±0.05	0.45	e
				0.375±0.088	0.58	d
^{56}Co	C	0.45±0.04	1.15±0.10			
^{58}Co	I	3.43±0.31	1.06±0.07			
^{60}Co	I	2.83±0.19	1.00±0.04			
^{65}Zn	C	4.08±0.25	1.03±0.04			
$^{69}Zn^{m}$	C	1.23±0.10	0.98±0.07			
^{74}As	I	2.48±0.20	1.01±0.08	1.2±0.4	0.45	e
				1.8±0.2	2.9	f
^{75}Se	C	5.18±0.33	1.00±0.03			
^{83}Rb	C	6.85±0.49	1.00±0.04	2.27±0.39	0.58	d
^{84}Rb	I	1.75±0.35	1.0 ±0.3	1.60±0.69	0.58	d
				1.7 ±0.4	29	g
^{83}Sr	C	3.21±0.32	1.05±0.11			

TABLE II. (continued)

Nuclide	Type of Yield[a]	$\sigma_{11.5}$ (mb)	$\sigma_{300}/\sigma_{11.5}$	Previous measurements σ (mb)	Ep (GeV)	Ref.
^{87}Y	C	7.1 ±0.5	1.02±0.05	0.70±0.18	0.58	d
^{89}Zr	C	5.46±0.36	1.03±0.04			
^{90}Nb	C	4.39±0.35	1.04±0.08			
^{95}Nb	C	0.83±0.09	0.93±0.10	1.90±0.26	0.58	d
^{96}Tc	I	2.58±0.17	1.00±0.04	0.59±0.26	0.58	d
^{103}Ru	C	0.41±0.04	0.85±0.12	0.97±0.08	0.58	d
^{100}Rh	I	2.5 ±0.5	1.0 ±0.3			
^{100}Pd	C	1.32±0.09	1.00±0.05			
^{105}Ag	C	5.0 ±0.4	1.01±0.08	0.475±0.099	0.58	d
$^{120}Sb^{m}$	I	0.16±0.03	1.0 ±0.3	0.150±0.017	18.2	c
^{121}Te	C	7.1 ±0.6	0.96±0.06			
$^{121}Te^{m}$	I	0.45±0.03	0.97±0.05			
^{122}Xe	C	7.8 ±0.6	0.95±0.10	7.6 ±0.5	29	g
^{127}Xe	C	9.5 ±0.6	0.96±0.03	9.6 ±0.6	3	g
				7.9 ±0.5	29	g
^{131}Ba	C	9.3 ±0.6	0.96±0.05	8.8 ±0.3	11.5	h
				8.3 ±0.7	300	h
^{133}Ba	C	8.8 ±0.8	0.93±0.10			
^{139}Ce	C	11.0±0.7	0.94±0.03	10.3±1.8[i]	28	j
^{143}Pm	C	9.8 ±0.6	0.92±0.03			
^{144}Pm	I	0.22±0.03	0.9 ±0.2			
^{145}Eu	C	13.0±0.8	0.94±0.04	6.65±0.06	28	j
^{147}Eu	C	14.3±1.0	0.93±0.05	10.9±0.9	28	j
^{148}Eu	I	0.58±0.06	1.0 ±0.2	1.20±0.25	28	j
^{149}Eu	C	17.7±2.0	0.89±0.15			

TABLE II. (continued)

Nuclide	Type of Yield[a]	$\sigma_{11.5}$ (mb)	$\sigma_{300}/\sigma_{11.5}$	Previous measurements σ (mb)	Ep (GeV)	Ref.
^{146}Gd	C	11.5±0.8	0.92±0.04	7.4 ±0.6	28	j
^{149}Gd	C	15.6±1.0	0.94±0.04	10.6±1.9[i]	28	j
^{167}Tm	C	15.5±1.1	0.95±0.04			
^{169}Yb	C	17.5±1.8	0.92±0.06			
^{170}Lu	C	19.1±1.3	0.95±0.04			
^{171}Lu	C	17.3±1.1	0.93±0.04			
^{173}Lu	C	20.5±1.3	0.93±0.04			
^{172}Hf	C	16.3±1.3	0.91±0.04			
^{175}Hf	C	17.7±1.1	0.88±0.04			
^{183}Re	C	20.6±1.3	0.94±0.05			
^{182}Os	C	19.0±2.0	- - - -			
^{183}Os	C	12.0±2.0	- - - -			
$^{183}Os^{m}$	C	10.0±1.7	- - - -			
^{185}Os	C	21.8±1.7	0.94±0.04			
^{188}Ir	I	6.5 ±1.1	1.2 ±0.3			
^{190}Ir	I	4.06±0.30	1.22±0.08			
^{192}Ir	I	2.45±0.16	1.21±0.06			
^{188}Pt	C	20.7±1.4	0.98±0.05			
^{194}Au	I	29.4±2.2	1.02±0.05			
^{196}Au	I	75 ±5	1.10±0.05	70.5±5.7	0.426	k

[a] C = cumulative, I = independent.

[b] Ref. 35.

[c] Ref. 37.

[d] Ref. 15.

[e] Ref. 32.

[f] Ref. 34.

[g] Ref. 36.

[h] Ref. 5.

[i] σ corrected to present γ-ray abundance.

[j] Ref. 38.

[k] Ref. 33.

TABLE III. Values for the parameters of equation (1)

Mass region	σ_o	P	R	S	T
$40 \leq A \leq 105$	7.8	-8.2×10^{-3}	$30\ A^{-0.79}$	0.470	2.1×10^{-4}
$120 \leq A \leq 185$	0.70	0.015	$6.5\ A^{-0.38}$	0.478	2.9×10^{-4}
Rudstam[a]		0.056	$11.8\ A^{-0.45}$	0.486	3.8×10^{-4}

[a]Ref. 52.

[1]S. Katcoff, S. B. Kaufman, E. P. Steinberg, M. W. Weisfield, and B. D. Wilkins, Phys. Rev. Lett. 30, 1221 (1973).

[2]G. English, Y. W. Yu, and N. T. Porile, Phys. Rev. Lett. 31, 244 (1973).

[3]G. English, N. T. Porile, and E. P. Steinberg, Phys. Rev. C10, 2268 (1974).

[4]G. English, Y. W. Yu, and N. T. Porile, Phys. Rev. C10, 2281, (1974).

[5]Y. W. Yu and N. T. Porile, Phys. Rev. C12, 938 (1975).

[6]S. K. Chang and N. Sugarman, Phys. Rev. C9, 1138 (1974).

[7]Y. W. Yu and N. T. Porile, Phys. Rev. C10, 167 (1974).

[8]Y. W. Yu, S. Biswas, and N. T. Porile, Phys. Rev. C11, 2111 (1975).

[9]G. E. Gordon, J. W. Harvey, and H. Nakahara, Nucleonics 24 (December), 62 (1966).

[10]D. J. Gorman and R. H. Tomlinson, Can. J. Chem. 46, 1663 (1968).

[11]G. R. Choppin and A. H. T. Kandil, J. Inorg. Nucl. Chem. 33, 897 (1971).

[12]B. Schrøder, G. Nydahl, and B. Forkman, Nucl. Phys. A143, 449 (1971).

[13]M. Areskoug, B. Schrøder, K. Lindgren, G. Andersson, and B. Forkman, Nucl. Phys. A226, 93 (1974).

[14]M. Areskoug, B. Schrøder, and K. Lindgren, Nucl. Phys. A251, 418 (1975).

[15]E. Ross and K. Bächmann, Radiochim. Acta 21, 13 (1974).

[16]B. R. Erdal and P. J. Karol, private communication.

[17]S. B. Kaufman and M. W. Weisfield, Phys. Rev. C11, 1258 (1975).

[18]S. B. Kaufman, M. W. Weisfield, and E. P. Steinberg, to be published.

[19]A. M. Poskanzer, G. W. Butler, and E. K. Hyde, Phys. Rev. C3, 882 (1971).

[20]R. G. Korteling, C. R. Toren, and E. K. Hyde, Phys. Rev. C7, 1611 (1973).

[21]J. Hudis and S. Tanaka, Phys. Rev. 171, 1297 (1968).

[22] J. R. Grover, Phys. Rev. 126, 1540 (1962).

[23] Y. W. Yu and N. T. Porile, Phys. Rev. C7, 1597 (1973).

[24] J. B. Cumming, Annu. Rev. Nucl. Sci. 13, 261 (1963).

[25] S. B. Kaufman, unpublished data.

[26] S. B. Kaufman, M. W. Weisfield, B. D. Wilkins, D. Henderson, and E. P. Steinberg, Phys. Rev. C13, 253 (1976).

[27] J. T. Routti and S. G. Prussin, Nucl. Instrum. Methods 72, 125 (1969); UCRL Report No. 19452, 1969 (unpublished).

[28] R. Gunnink and J. B. Niday, UCRL Report No. 51061, 1972 (unpublished).

[29] J. B. Cumming, National Academy of Sciences Report No. NAS-NS-3107, 1962 (unpublished), p. 25.

[30] Nuclear Data Sheets 16, 267 (1975).

[31] R. M. Diamond, J. M. Hollander, D. J. Horen, and R. A. Naumann, Nucl. Phys. 25, 248 (1961).

[32] P. Kruger and N. Sugarman, Phys. Rev. 99, 1459 (1955).

[33] H. P. Yule and A. Turkevich, Phys. Rev. 118, 1591 (1960).

[34] S. B. Kaufman, Phys. Rev. 129, 1866 (1963).

[35] J. Hudis and S. Tanaka, Phys. Rev. 171, 1297 (1968).

[36] J. Hudis, T. Kirsten, R. W. Stoenner, and O. A. Schaeffer, Phys. Rev. C1, 2019 (1970).

[37] E. Hagebø and H. Ravn, J. Inorg. Nucl. Chem. 31, 897 (1969).

[38] K. Bächmann, J. Inorg. Nucl. Chem. 32, 1 (1970).

[39] P. L. Jain, M. Kazumo, G. Thomas, and B. Girard, Phys. Rev. Lett. 33, 660 (1974); P. L. Jain, B. Girard, M. Kazumo, and G. Thomas, Phys. Rev. Lett. 34, 972 (1975).

[40] Barcelona-Batavia-Belgrade-Bucharest-Lund-Lyons-Montreal-Nancy-Ottawa-Paris-Rome-Strasbourg-Valencia Collaboration, Phys. Lett. 48B, 467 (1974).

[41] W. Busza, J. E. Elias, D. F. Jacobs, P. A. Swartz, C. C. Young, and M. R. Sogard, Phys. Rev. Lett. 34, 836 (1975).

[42] W. Busza, in High-Energy Physics and Nuclear Structure - 1975, (American Institute of Physics, New York, N. Y., 1975), p. 211.

[43] K. Gottfried, Phys. Rev. Lett. 32, 957 (1974).

[44] Ø. Scheidemann and N. T. Porile, to be published.

[45] R. Wolfgang, E. W. Baker, A. A. Caretto, J. B. Cumming, G. Friedlander, and J. Hudis, Phys. Rev. 103, 394 (1956).

[46] V. P. Crespo, J. M. Alexander and E. K. Hyde, Phys. Rev. 131, 1765 (1963).

[47] G. N. Simonoff and C. Vidal, Phys. Lett. 20, 30 (1966).

[48] G. Friedlander, L. Friedman, B. Gordon, and L. Yaffe, Phys. Rev. 129, 1809 (1963).

[49] K. Beg and N. T. Porile, Phys. Rev. C3, 1631 (1971).

[50] L. Winsberg, Phys. Rev. 135, B1105 (1964); E. M. Franz and G. Friedlander, Nucl. Phys. 76, 123 (1966).

[51] J. Hudis and S. Katcoff, Phys. Rev. 180, 1122 (1969).

[52] G. Rudstam, Z. Naturforsch. 21a, 1027 (1966).

[53] Y. Y. Chu, E. M. Franz, and G. Friedlander, Phys. Rev. C10, 156, (1974).

[54] G. Friedlander, in Proceedings of the Symposium on the Physics and Chemistry of Fission, Salzburg, Austria, 1965 (IAEA, Vienna, Austria, 1965), Vol. II, p. 265.

[55] J. A. Panontin and N. T. Porile, J. Inorg. Nucl. Chem. 33, 3211 (1971).

Fig. 1. Ratio of cross sections at the two bombarding energies, $\sigma_{300}/\sigma_{11.5}$, as a function of mass number. Open symbols are neutron deficient nuclides, solid symbols are neutron-excess nuclides. (o,●): cumulative cross sections; (□,■): independent cross sections; (▽): Ref. 5.

Fig. 2. Charge dispersion curves calculated for specific mass numbers from Eq. (1). Open symbols are independent yields, solid symbols cumulative yields. (o,●): this work; (□,■): Ref. 37; (◆): Ref. 36.

Fig. 3. Charge dispersion curves calculated for specific mass numbers from Eq. (1). Open symbols are independent yields, solid symbols cumulative yields. (o,●): this work; (▽,▼): Ref. 5; (Δ,▲): Ref. 38. The dashed curves show the cumulative yields from positron/electron-capture decay.

Fig. 4. (a) Variation of parameter R of Eq. (1) with mass number Full lines: this work; dashed line: Rudstam (Ref. 52). (b) Variation of Zp/A with mass number. Full lines: this work; dashed line: Rudstam (Ref. 52); dotted curve: beta-stable nuclides.

Fig. 5. Mass-yield curve for 11.5-GeV protons + ^{197}Au. (●): cumulative cross sections, including data from Ref. 5; (o) independent cross sections; (x): total isobaric cross sections at 29 GeV (Ref. 36). The full lines are calculated from Eq. (1) and the dashed lines represent likely extrapolations.

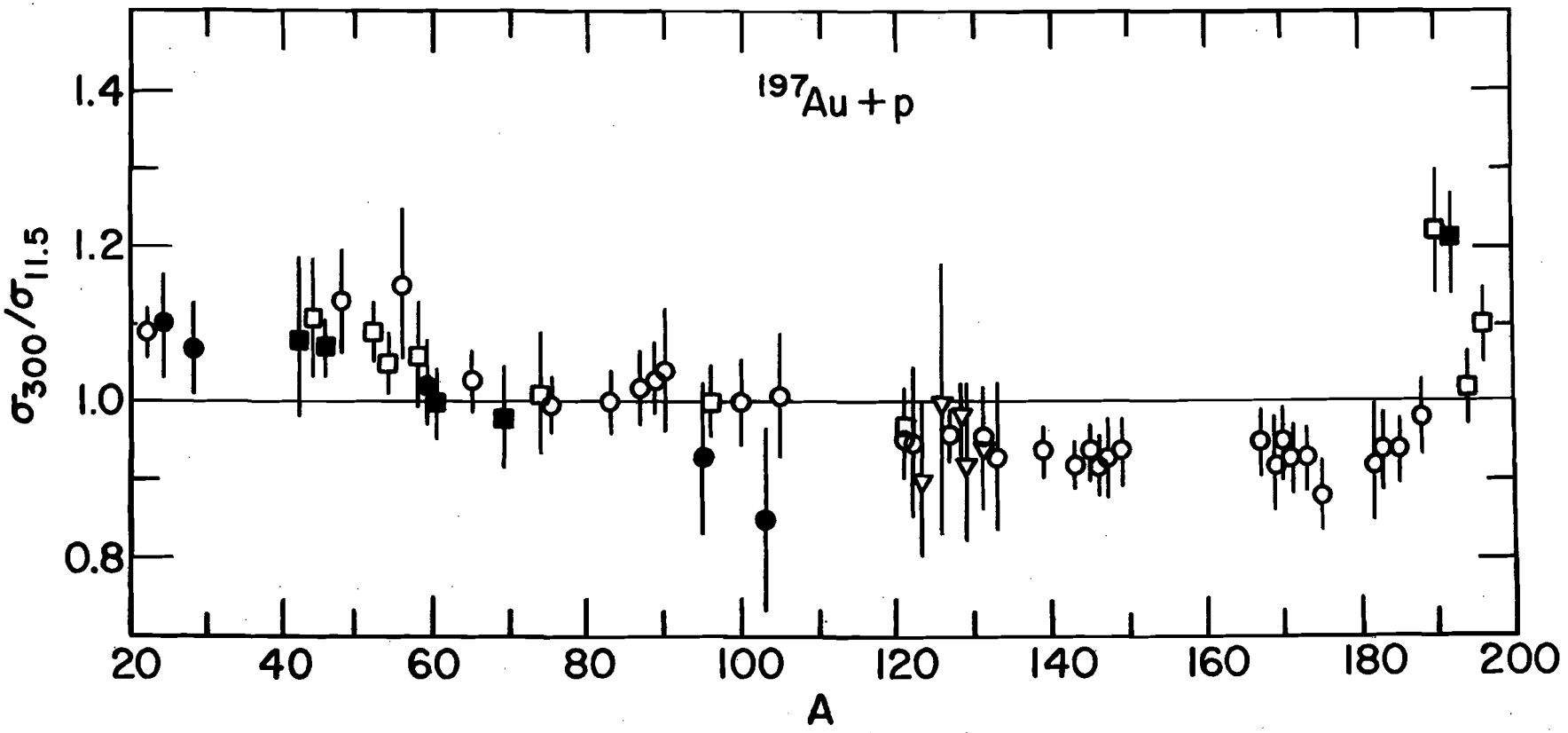
^{197}Au + p
$\sigma_{300}/\sigma_{11.5}$
1.4
1.2
1.0
0.8
20
40
60
80
100
120
140
160
180
200
A

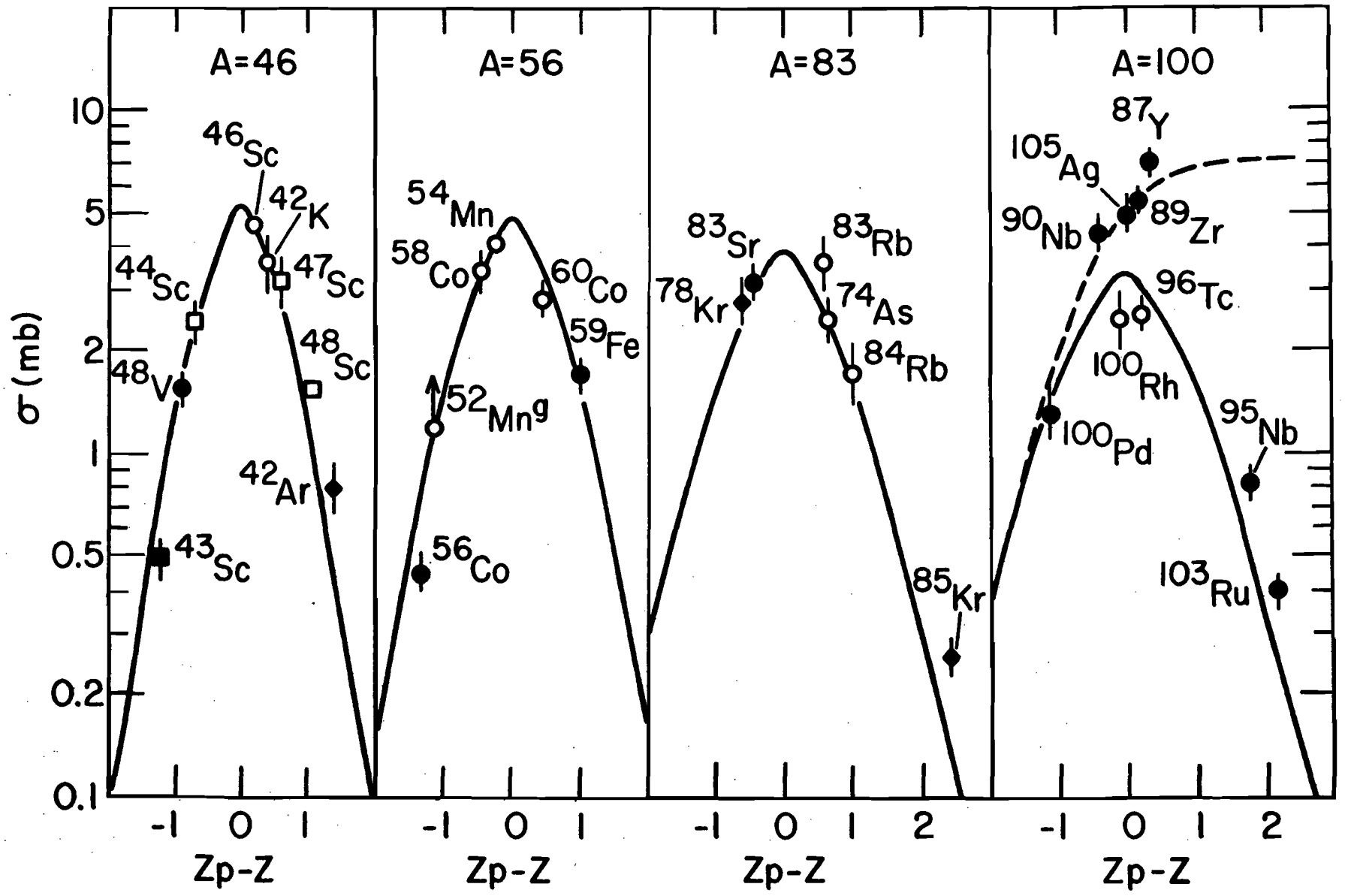
A=46
A=56
A=83
A=100
σ (mb)
10
5
2
1
0.5
0.2
0.1
46Sc
42K
44Sc
47Sc
48Sc
48V
42Ar
43Sc
54Mn
58Co
60Co
59Fe
52Mng
56Co
83Sr
83Rb
78Kr
74As
84Rb
85Kr
87Y
105Ag
90Nb
89Zr
96Tc
100Rh
100Pd
95Nb
103Ru
-1
0
1
2
Zp-Z

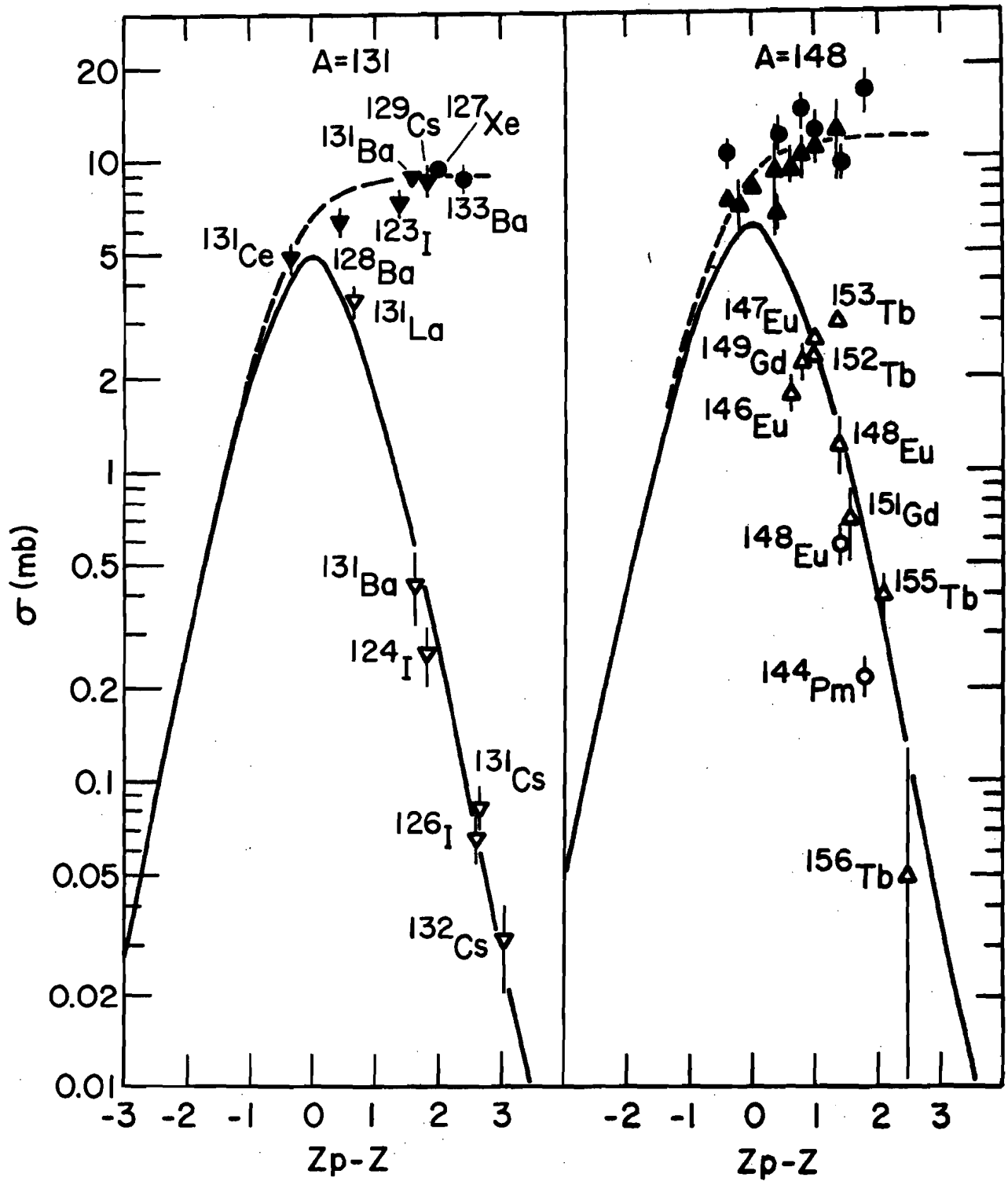
A=131
A=148
σ (mb)
Zp-Z
Zp-Z
129Cs
127Xe
131Ba
133Ba
123I
131Ce
128Ba
131La
131Ba
124I
131Cs
126I
132Cs
147Eu
153Tb
149Gd
152Tb
146Eu
148Eu
151Gd
148Eu
155Tb
144Pm
156Tb

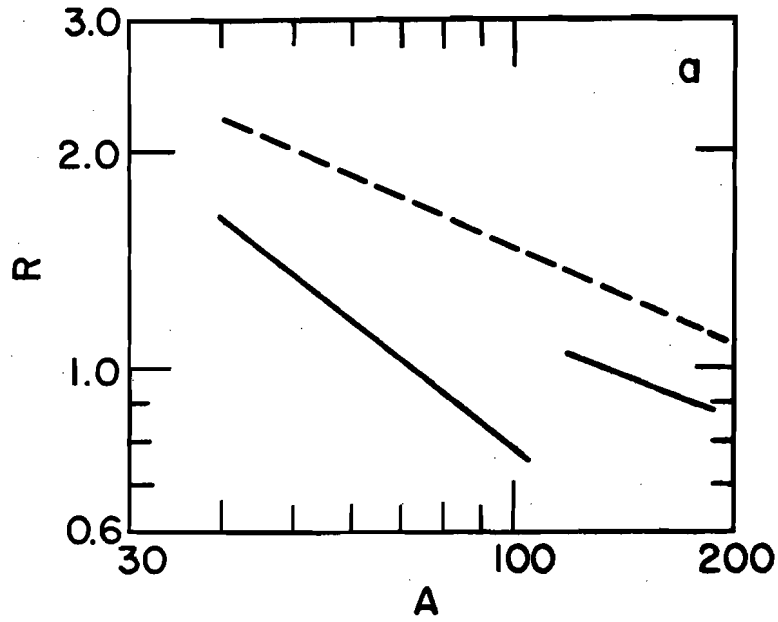
3.0
2.0
1.0
0.6
R
a
30
100
200
A

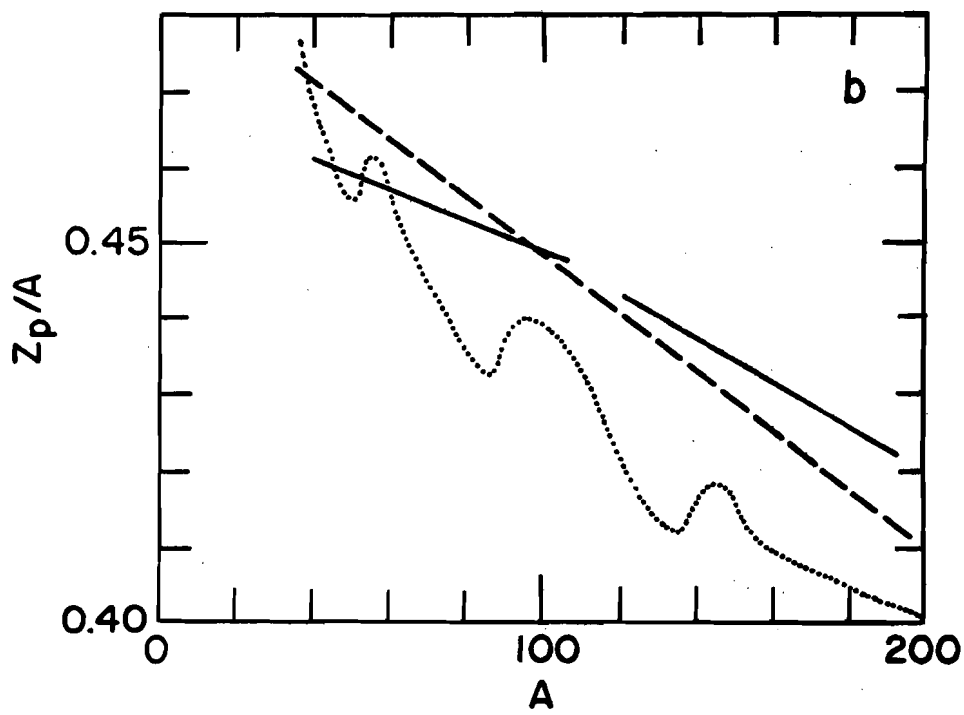
0.45
0.40
Zp/A
b
0
100
200
A

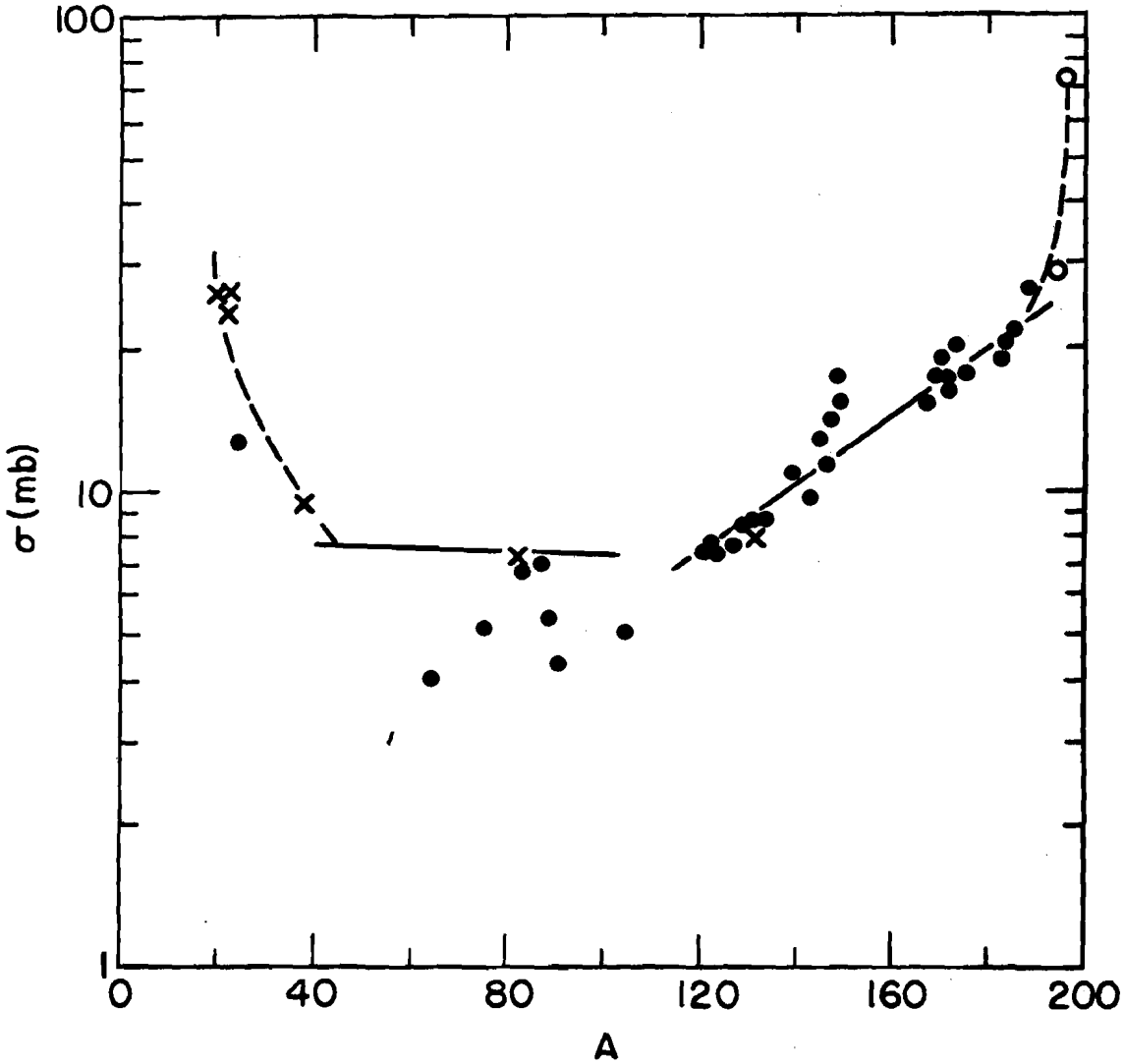
100
10
1
σ (mb)
0
40
80
120
160
200
A